ACS OMEGA

http://pubs.acs.org/journal/acsodf

Article

Effect of Synergistic Modification of Building Materials Based on α-Hemihydrate Phosphogypsum by Portland Cement/H-PDMS on Water Resistance

Guang Yang, Lei Deng, Xiaofeng Luo, and Qibin Liu*

Cite This: *ACS Omega* 2022, 7, 41667−41677

Read Online

ACCESS | Metrics & More | Article Recommendations

ABSTRACT: Alpha-hemihydrate phosphogypsum (α-HPG) is a cementitious material obtained by dehydration of phosphogypsum (PG), a byproduct of phosphoric acid production. Poor water resistance of α-HPG has usually restricted its application in construction materials. In this study, hydroxy-terminated polydimethylsiloxane (H-PDMS) and Portland cement (PC) were used for the hydrophobic modification of α-HPG. The fluidity, setting times, compressive strength, flexural strength, ratio of compressive to flexural strength, water absorption rate, softening coefficient, pore structure, chemical information, and microstructure of the samples were measured to evaluate the modification effect of H-PDMS and PC. The results showed that H-PDMS and PC significantly improved waterproof properties of α-HPG and reduced its porosity, total pore area, and pore diameter. Specifically, PC provided the reactive group −OH that reacted with H-PDMS. Also, due to the coverage of hydrophobic $-CH_3$ groups, PG was given an overall hydrophobicity with a contact angle of 134° (1.5% H-PDMS). H-HPG (H-PDMS- and PC-modified α-HPG) hydrophobic material can be used in building materials with waterproof requirements and achieve the comprehensive utilization of solid waste PG.

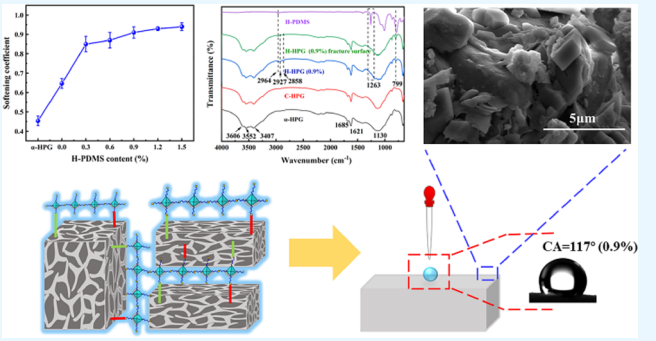

1. INTRODUCTION

Phosphoric acid is an essential raw material for the production of phosphate fertilizers.[1] In recent years, as the output of phosphoric acid has increased year by year, phosphogypsum (PG), as a solid waste produced when the industrial use of sulfuric acid to decompose phosphate rock to produce phosphoric acid, has also greatly increased its emissions.[2] Typically, 4.5−5.5 tons of PG solid waste is generated for every 1 ton of phosphoric acid produced. According to statistics, the cumulative global emission of PG is about 6 billion tons, and it is increasing at a rate of 150 million tons per year.[3] At present, the annual production of PG in the world exceeds 300 million tons, and the overall comprehensive utilization rate of resources is about 10%.[4] The discharge and storage of PG not only occupy a lot of land resources and increase the processing cost of enterprises but also seriously damage the ecological environment due to the large accumulation of PG with its complex composition.[5] Therefore, how to utilize PG resources is still a major problem.

Hemihydrate phosphogypsum (HPG) is obtained by dehydrating the original PG (PG), and its main chemical component is calcium sulfate hemihydrate ($CaSO_4 \cdot 0.5H_2O$). By different preparation methods, two types of PG can be formed: alpha-hemihydrate phosphogypsum (α-HPG) and beta-hemihydrate phosphogypsum (β-HPG). Compared with β-hemihydrate PG, α-hemihydrate phosphogypsum has the characteristics of high crystallinity, low heat of hydration, low water demand, and high strength of a hardened body. Therefore, using the above characteristics of α-hemihydrate phosphogypsum, it is hydrophobically modified to prepare a widely available PG block, which provides a new idea for reducing ecological environment pollution and improving the utilization rate of phosphogypsum.[6]

The modification of inorganic cementitious materials can significantly improve the mechanical properties and water resistance of gypsum, which is one of the effective methods for the modification of industrial byproduct phosphogypsum.[7] Jin et al.[8] used calcium sulfoaluminate cement to significantly improve the mechanical strength and water resistance of β-hemihydrate phosphogypsum. Ma et al.[9] studied the effects of single and composite doping of fluidized bed ash and cement on the

Received: September 1, 2022
Accepted: October 25, 2022
Published: November 4, 2022

mechanical properties and water resistance of phosphogypsum. The optimum admixture of cement, fluidized bed ash, and phosphogypsum was determined by ANOVA. Meskini et al.[10] prepared a mixture of phosphogypsum and fly ash, which was then activated with different lime additions to form different combinations. The effects of curing time and mixture composition on the mineralogy of the composites were investigated to emphasize the effect of calcium alumina as the main hydration product on strength development.

Geopolymer is an aluminosilicate material with a three-dimensional amorphous structure formed by alkali-excited active aluminosilicate minerals, and the reaction process is called alkali-excited geopolymerization.[11,12] Compared with the current common utilization methods, the comprehensive utilization of phosphate mine solid waste by the alkali-excited geopolymerization reaction is a new sustainable method that can treat phosphorus tailings, phosphogypsum, and yellow phosphorus slag in a low-cost and environment-friendly way, which can turn them into treasures and improve the comprehensive utilization rate of phosphate mine solid waste.[13−16] Geopolymer is an environmentally friendly cementitious material with good mechanical properties, which can dissipate a large amount of solid waste and is used in different fields as a substitute for ordinary silicate cement.[17,18] Li et al.[19] investigated the effects of blending gypsum dihydrate, flue gas desulfurization gypsum, and phosphogypsum on the compatibility and mechanical properties of red mud slag slurry materials with different gypsum contents. Shi et al.[20] added modified quartz sand to the phosphogypsum cementitious filling slurry, which can effectively improve the phosphate contamination in the process of phosphogypsum cementation and filling.

The hydrophobic admixture method uses the hydrophobic modifier as an admixture for PG to obtain the overall hydrophobicity, which is added during the mixing process of the hemihydrate PG and water. Wu et al.[21] prepared a silane-modified benzene propylene emulsion to form a strong hydrophobic film on the surface of desulfurization gypsum crystals, which improved the waterproof performance and softening coefficient denseness of desulfurization gypsum products and reduced the porosity of the structure. Li et al.[22] mixed silicone oil paraffin emulsion and nano-silica into desulfurization gypsum to improve its waterproof and mechanical properties. Wang et al.[23] studied the effect of three different emulsions on the water repellency and mechanical properties of flue gas desulfurization calcined gypsum. As an eco-friendly cementitious material obtained from original PG, the main problems for the utilization of α-HPG are still the poor waterproof properties. However, single organic hydrophobic admixture or inorganic cementitious materials' method cannot achieve good results.

In this study, organic hydrophobic admixture and inorganic cementitious material Portland cement were combined to improve water resistance of α-HPG. Portland cement acted as a bridge to provide the −OH groups required for the reaction, filling the voids between the PG crystals and hydrated with the PG to form ettringite. Hydroxy-terminated polydimethylsiloxane (H-PDMS) was selected as a hydrophobic modifier, reacting with the hydroxyl groups on the surface of phosphogypsum−cement composite to endow the phosphogypsum-based building block with integral hydrophobicity. To the best of our knowledge, a large number of superhydrophobic coatings based on PDMS have been reported.[24,25] However, the use of H-PDMS as a phosphogypsum-based building material hydrophobic additive has not been reported so far.

The compressive strength, flexural strength, and ratio of compressive to flexural strength were measured to determine the mechanical strength of the waterproof block. The water absorption rate and softening coefficient were measured to determine the waterproof properties of the waterproof block. The purpose of this study is to optimize the properties of H-PDMS-modified phosphogypsum-based building materials and achieve the effective utilization of PG.

2. MATERIALS AND METHOD

2.1. Materials. α-HPG used in this study was obtained from Wengfu (Group) Co., Ltd. (China), which has been harmlessly pre-treated. The X-ray diffraction (XRD) pattern of α-HPG is shown in Figure 1. The particle size distribution of α-HPG and

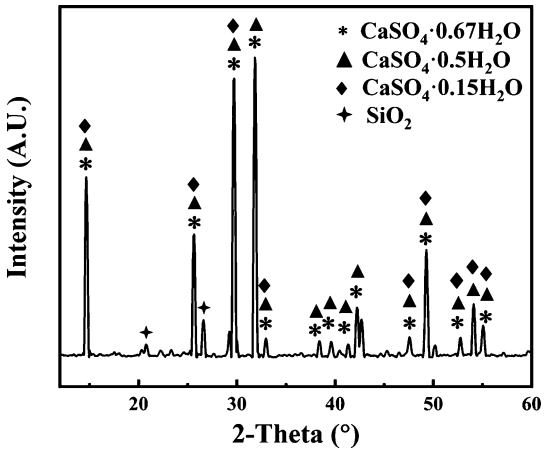

Figure 1. XRD spectrum of α-HPG.

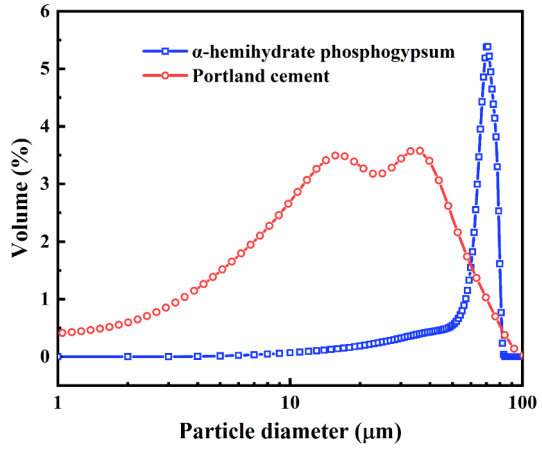

Figure 2. Particle size distributions of α-HPG and PC.

PC are shown in Figure 2. The particle size of α-HPG ranged from 0.04 to 92.0989 μm, and the mean particle size (d50) of which was 23.41 μm. The particle size of Portland cement ranges from 0.04 to 110.987 μm, and the mean particle size (d50) of which was 15.86 μm. The main crystal phases in α-HPG were $CaSO_4{\cdot}0.5H_2O$ and SiO_2 (Figure 1). The chemical compositions of α-HPG are presented in Table 1, indicating that α-HPG contains 90.12 wt % $CaSO_4{\cdot}0.5H_2O$ (calculated from the

https://doi.org/10.1021/acsomega.2c05662
ACS Omega 2022, 7, 41667−41677

Table 1. α-Hemihydrate Phosphogypsum Composition

composition	content/wt %
SO_3	52.37
CaO	37.75
SiO_2	5.66
F	1.85
P_2O_5	1.04
Al_2O_3	0.63
Fe_2O_3	0.15
Na_2O	0.15
K_2O	0.13
SrO	0.07
BaO	0.07
Cl	0.05
In_2O_3	0.04
TiO_2	0.04

contents of SO_3 and CaO) and small amounts of SiO_2, P_2O_5, and Al_2O_3. Radionuclides and soluble heavy metals in α-HPG can cause environmental problems, restricting its use in building materials. The contents of heavy metals (Pb, Cd, Cr, and Hg) of α-HPG were all lower than the limit values of the Chinese standard (GB18582-2008) (Table 2).

Table 2. Soluble Heavy Metals in α-HPG

	demand of standards	test results
heavy metals	Pb ≤ 90 mg/kg	Pb = 6.97 mg/kg
	Cd ≤ 90 mg/kg	Cd = 0.93 mg/kg
	Cr ≤ 90 mg/kg	Cr = 16.73 mg/kg
	Hg ≤ 90 mg/kg	Hg = 0.93 mg/kg

Portland cement (PO 42.5) was provided by Jiangxi Fenyi Conch Cement Co., Ltd. (China). Polyester fiber with a length of 6 mm and a diameter of 20 μm ± 4 μm was provided by Changsha Ningxiang building materials Co. Ltd. (China). H-PDMS (viscosity 1800−2200 cSt) was purchased from Sigma-Aldrich. Tetraethoxysilane (TEOS) and dibutyl dilaurate, used as the curing agent and accelerator, respectively, were purchased from Shanghai Aladdin Biochemical Technology Co., Ltd.

2.2. Preparation of Samples. α-HPG, Portland cement, and tap water were blended in a cement mortar mixer (JJ-5, China) for 2 min (all the raw materials were mixed according to the designed mix proportions, Table 3, and all samples were added with 0.3% wt polyester fiber to improve the flexural strength of the PG blocks. Combining water resistance and strength factors, it was determined that the optimum dosage of Portland cement was 10%). 95 wt % H-PDMS, 5 wt % TEOS, and 1 wt % dibutyl dilaurate were manually mixed in a mixing vessel for 1 min to prepare the H-PDMS hydrophobic agent. Afterward, the liquid mixture of H-PDMS agent was poured into the mixer. The mixture was further blended at a high speed for 1 min to ensure the homogeneous dispersion of H-PDMS in the phosphogypsum−cement mortar. Specimens with the size of 40 mm × 40 mm × 160 mm were molded at natural conditions for 24 h, then demolded and cured for 7 days at the same environment for the tests of mechanical strength.

Table 3. Mixture Component

	mix proportions (wt %)		
no.	α-HPG	Portland cement	H-PDMS waterproofing agent
P1	100	0	0
P2	90	10	0
P3	90	10	0.3
P4	90	10	0.6
P5	90	10	0.9
P6	90	10	1.2
P7	90	10	1.5

The dosage of H-PDMS in the hardened α-HPG was 0, 0.3, 0.6, 0.9, 1.2, and 1.5 wt % (by α-HPG weight). The unmodified HPG, Portland cement-modified HPG, and H-PDMS/Portland cement-modified HPG samples were denoted as α-HPG, C-HPG, and H-HPG, respectively.

2.3. Sample Characterization. *2.3.1. Fluidity and Setting Time.* The fluidity and setting times of different samples were measured according to GB/T17669.4-1999.

2.3.2. Mechanical Strength Measurement. The mechanical strength of specimens was measured using a fully automatic test machine (DYE-300S, China) in accordance with the Chinese standard (GB/T 17669.3-1999). The loading rate of the compressive strength and flexural strength tests were 2400 and 50 N/S, respectively.

2.3.3. Surface Wettability Analysis. The sample was polished with 240# sandpaper to remove impurities and construct a desired roughness on the surface of PG. The CA of different sample surfaces was measured using an optical contact angle tester (JC2000D1, China).

2.3.4. Water Absorption Measurement and Softening Coefficient. Specimens after curing were dried at the temperature of 45 ± 5 in an electric thermostatic drying oven until the weight was constant and then soaked in water to absorb water. Three specimens were prepared for each mix proportion. The water absorption rate was calculated as

$$\omega = \frac{m_2 - m_1}{m_1} \times 100\% \quad (1)$$

where m_1 (g) is the mass of the specimen before soaking in water and m_2 (g) is the mass of the specimen after soaking in water.

The softening coefficient was calculated as

$$K = \frac{f}{F} \quad (2)$$

where F (MPa) is the dry compressive strength of the specimen and f (MPa) is the compressive strength of the specimen after soaking in water.

2.3.5. XPS Analysis. For the surface analysis, X-ray photoelectron spectrometry (XPS) spectra were acquired with a Thermo Scientific K-Alpha instrument, using an Al Kα source ($h\nu$ = 1486.6 eV).

2.3.6. Pore Structure Measurement. The pore structure was measured using a mercury intrusion porosimeter (MIP, AutoPore Iv 9510). The measuring range of aperture was from 5 nm to 800 μm. Samples were freeze-dried at −50 °C for 24 h to remove water of crystallization before the test.

2.3.7. SEM Analysis. Scanning electron microscope (HITACHI SU8100, Japan) was used to investigate the microstructure of specimens. The test was carried out with an accelerating voltage of 10−15 kV and a working distance of 10 mm in high vacuum mode.

2.3.8. ATR-FTIR Analysis. The structural information of the organic components was analyzed using an attenuated total reflection Fourier transform infrared spectrometer (Nicolet iS50, USA).

https://doi.org/10.1021/acsomega.2c05662
ACS Omega 2022, 7, 41667−41677

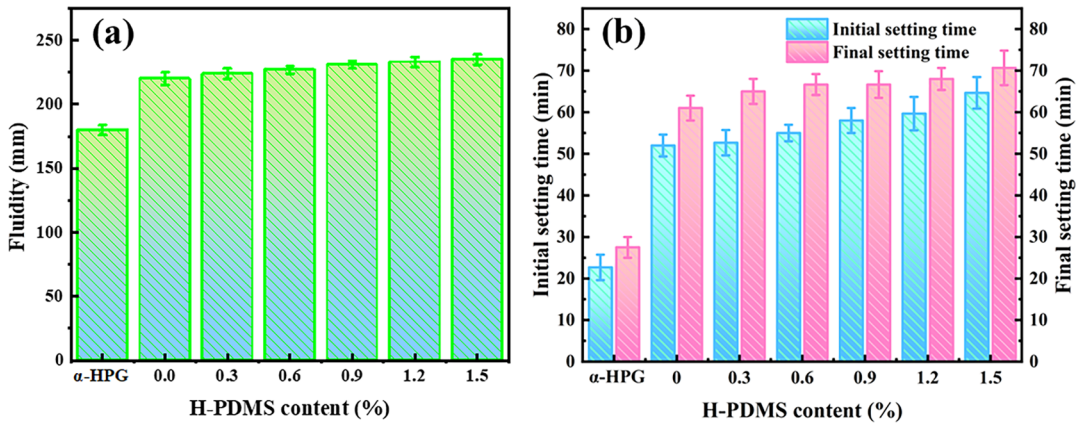

Figure 3. Effects of the H-PDMS contents on (a) fluidity and (b) initial and final setting times.

3. RESULTS AND DISCUSSION

3.1. Variation in Fluidity and Setting times. It is shown in Figure 3a, that the fluidity of samples increases greatly when 10% of cement is added (0% H-PDMS content) because the water demand for cement is less than that of hemihydrate PG. The fluidity of the HPG sample is slightly improved after the modification of H-PDMS. The higher the content of H-PDMS, the better the fluidity of HPG. This phenomenon can be explained by the fact that liquid H-PDMS plays the role of lubricant in HPG. With increasing H-PDMS content in the HPG sample, the fluidity of HPG increases further, indicating that the higher the H-PDMS content, the stronger the lubrication effect.

Figure 3c shows that the setting times of the cement−HPG system increases with 10% cement added because the setting time of cement is longer than hemihydrate PG. Both the initial and final setting times of the H-PDMS-modified HPG are slightly improved with increasing H-PDMS content by adsorption on the surface of the crystals. However, H-PDMS agent does not affect the crystallization and growth of the gypsum crystals.

3.2. Mechanical Properties. The mechanical strength of specimens with different contents of H-PDMS is shown in Figure 4. The compressive strength of specimens with the H-PDMS content ranging from 0 to 1.5% is decreased by 3.98, 10.18, 13.27, 17.26, 22.12, and 33.63%, respectively, compared to the α-HPG specimen. The flexural strength of specimens decrease with the decrease of compressive strength, decreasing by 33.33, 33.33, 35.36, 33.33, 35.56, and 40.00%, respectively.

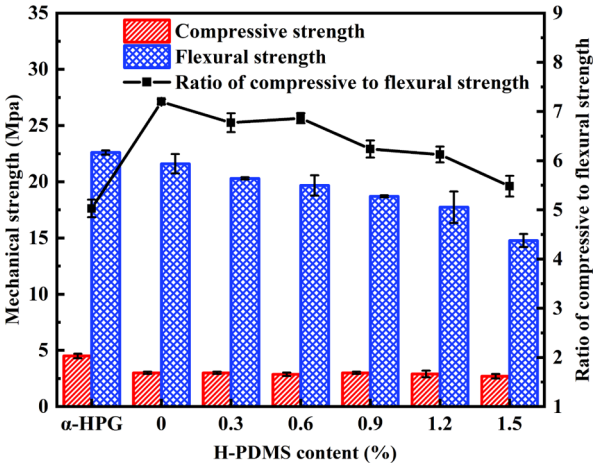

Figure 4. Mechanical strength of specimens with different contents of H-PDMS.

The ratio of compressive to flexural strength is used to evaluate the flexibility of materials, and the flexibility decreases with the increase of the ratio of compressive to flexural strength.[26] Portland cement is a kind of cementitious material with lower flexibility due to its hydration products.[27] When the contents of H-PDMS are 0%, the addition of 10% Portland cement affects the hydration of α-HPG and forms hydration products with lower flexibility, so the increase of the ratio of compressive to flexural strength is about 44.02%. With the increase of H-PDMS content, the ratio of compressive to flexural strength declines steadily compared with C-HPG added 10% Portland cement, but always higher than the ratio of α-HPG. The result indicates that the modification of H-PDMS will increase the toughness of the phosphogypsum-based composites.

3.3. Water Absorption Analysis and Softening Coefficients of Different Mixtures. The water absorption rate and softening coefficient are indexes to evaluate the waterproof properties of solid materials. Figure 5 shows the water absorption rate and softening coefficient of specimens with different contents of H-HPG. The water absorption rates of specimens decreased significantly with the increasing content of H-PDMS. Compared to the reference specimen α-HPG without the addition of H-HPG and Portland cement, the water absorption rates decreased by 10.56, 79.59, 82.59, 84.39, 84.63, and 84.99% with the H-PDMS contents ranging from 0 to 1.5 wt %. The softening coefficients of specimens increase with the addition of H-PDMS. When the contents of H-PDMS range from 0 to 1.5 wt %, the softening coefficients of specimens are increased by 44.12, 88.89, 93.33, 102.22, 106.67, and 108.89%, respectively.

Especially when the contents are over 0.9 wt %, the softening coefficients of specimens are over 0.91, which shows good performance of waterproof properties. The decrease of the water absorption rate and increase of softening coefficient of specimens indicate that the pore structure and hydration products of hardened PG are changed under the effect of Portland cement and H-PDMS. The synergistic effect of H-PDMS and Portland cement can improve the water absorption rates and softening coefficient of α-HPG simultaneously, and the effect becomes more dominant as the content of H-PDMS increases.

https://doi.org/10.1021/acsomega.2c05662
ACS Omega 2022, 7, 41667−41677

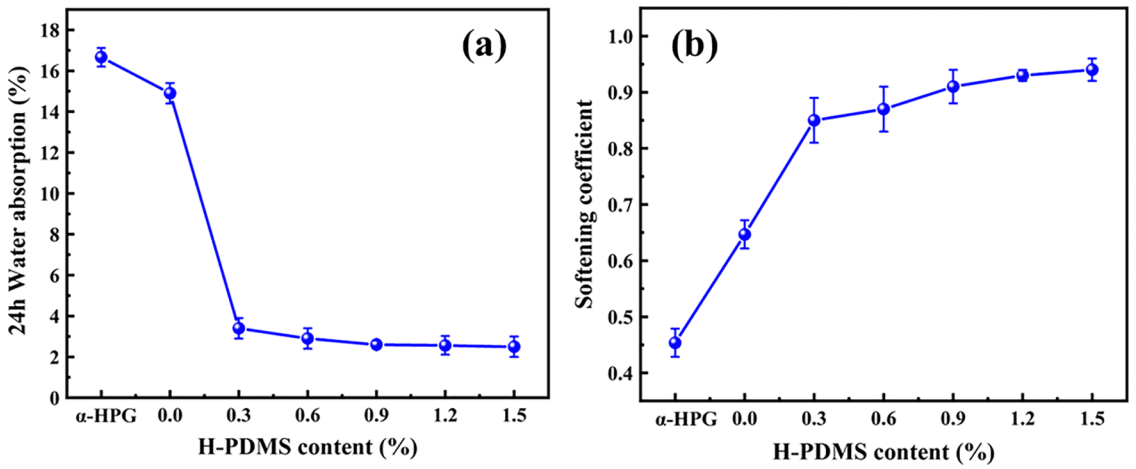

Figure 5. (a) Water absorption rates and (b) softening coefficients of different samples.

3.4. Surface Wettability of Different HPG Surfaces.

Figure 6 shows the effect of the H-PDMS content on the surface wettabilities of different HPG samples. The surface of α-HPG and C-HPG are hydrophilic (CA = 0°). The CA of the H-HPG surface increases apparently with increasing H-PDMS content. The surface of the H-HPG containing 1.2 wt % H-PDMS exhibits a CA of 124°, demonstrating its hydrophobicity. In addition, when the content of H-PDMS increases to 1.5 wt %, the CA of the H-HPG surface does not change much. Therefore, the H-HPG sample modified with 0.9 wt % H-PDMS is used for further characterization.

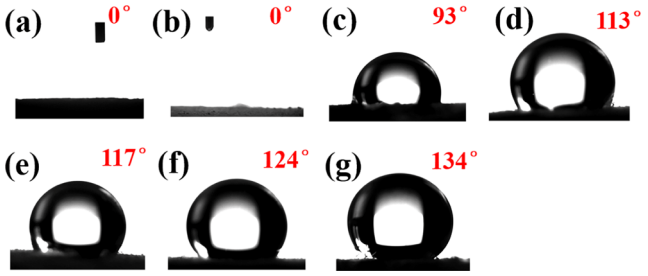

Figure 6. Effect of H-PDMS content on the contact angle of water with different HPG surfaces. (a) α-HPG; (b) C-HPG; (c) H-HPG, 0.3%; (d) H-HPG, 0.6%; (e) H-HPG, 0.9%; (f) H-HPG, 1.2%; and (g) H-HPG, 1.5%.

Figure 7a,b shows a drop of water penetrating into the pores of the α-HPG and C-HPG surfaces, and the obtained CA value is 0°, indicating their hydrophilic nature. As a comparison, the water droplet showing spherical shape sits on the H-HPG surface, which is hydrophobic (Figure 7c,d, water is dyed with methylene blue for good observation). Figure 7d also shows that larger water droplets could can still retain their shape without being sucked in by the H-HPG surface easily. Particularly, the newly exposed abrasion surface and fractured surface (after being destroyed) of H-HPG are also hydrophobic (Figure 7e,f), demonstrating the bulk hydrophobicity of the H-HPG.

Figure 8a shows that after being immersed in water, C-HPG and α-HPG without H-PDMS modification quickly become darker due to a large amount of water absorption in a short period of time. However, the phosphogypsum modified by H-PDMS still has a light gray-white color due to its hydrophobicity. H-PDMS-modified HPG samples, from 0.3 to 1.5%, all exhibit a mirror-like phenomenon after it is immersed into water by taking the H-HPG (0.9%) (see Figure 8b) as an example. Also, the surface is completely dried after it is taken out of the water.

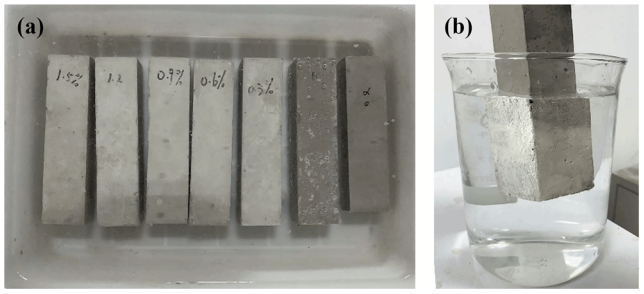

Figure 8. (a) Immersion experiment and (b) submerging test. Mirror-like surface forms, example of H-HPG, 0.9%.

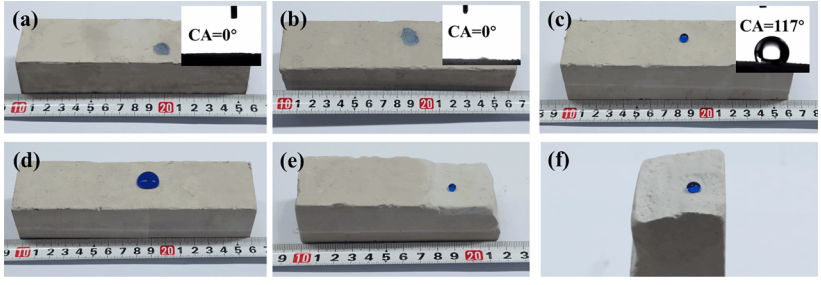

Figure 7. Images of water droplets on different HPG surfaces. (a) α-HPG surface; (b) C-HPG surface; (c) surface of H-HPG, 0.9%; (d) larger droplet surface of H-HPG, 0.9%; (e) abrasion surface of H-HPG, 0.9%; and (f) fractured surface of H-HPG, 0.9%.

https://doi.org/10.1021/acsomega.2c05662
ACS Omega 2022, 7, 41667−41677

The mirror-like phenomenon is attributed to an air layer formed between the hydrophobic H-PDMS surface and water.[28]

3.5. XPS Analysis. To further explore the influence mechanism of the H-PDMS (including the curing agent and the accelerator) on the water resistance performance of the phosphogypsumcement system, XPS is carried out by selecting four samples: H-PDMS agent, α-HPG, C-HPG, and H-HPG (0.9%). Figure 9 shows the total XPS spectrum of the elements in the gypsum samples, and the content of each element is presented in Table 4.

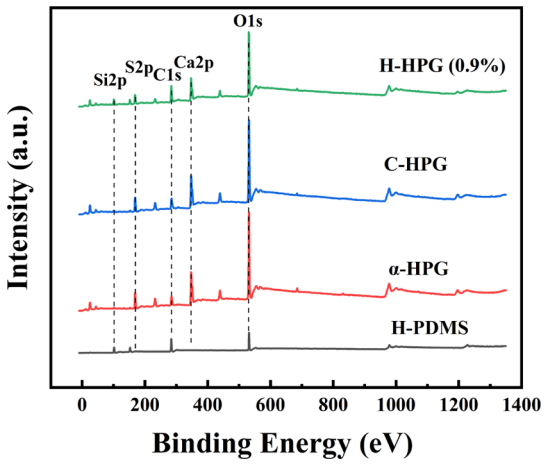

Figure 9. Total XPS spectrum of the gypsum sample.

Table 4. Contents of Each Element in Phosphogypsum Samples

sample	C 1s/%	Ca 2p/%	O 1s/%	S 2p/%	Si 2p/%
H-HPG (0.9%)	27.8	8.46	47.62	7.85	8.27
C-HPG	18.50	11.71	56.05	10.97	2.76
α-HPG	17.41	11.69	56.3	12.55	2.05
H-PDMS	50.37		23.98		24.5

Both the XPS spectra in Figure 9 and the element content in Table 4 show that the main elements of the H-PDMS agent are C, Si, and O, and that Si and O account for 24.5 and 23.98% of the substance, respectively, indicating that the hydrophobic agent contained a large number of Si−O bonds and −OH.

The main elements in the α-HPG, C-HPG, and H-HPG (0.9%) are O, C, S, Ca, and Si. Compared with the α-HPG and C-HPG, the content of Si and C of H-HPG (0.9%) increases more significantly, indicating that the H-PDMS hydrophobic network is adsorbed onto the surface of the gypsum crystal, which is conducive to the improvement of the water resistance of phosphogypsum.

In the XPS results, the changes in Si 2p and the peak fitting of O 1s in the α-HPG, C-HPG, and H-HPG (0.9%) are shown in Figure 10. Figure 10a shows that the addition of the H-PDMS agent significantly increases the relative content of silicon in gypsum compared with that of the phosphogypsum reference group. This is because the H-PDMS agent used is an organosilicon hydrophobic agent, and silicon is its main element. On the basis of cement addition (C-HPG), the addition of the H-PDMS agent shifted the peak position of the silicon peak in the gypsum to lower binding energy, indicating that a chemical reaction occurred between the H-PDMS hydrophobic agent and the phosphogypsum−cement, changing the binding state of silicon within the XPS spectrum of H-HPG. The relative content of Si 2p is higher, and the peak position shift is more obvious, indicating that Portland cement hydration provides phosphogypsum with reactive groups and appropriate alkalinity, to which the addition of H-PDMS can better promote the chemical reaction between them.[29]

Figure 10b−d shows the peak fitting results of the O 1s XPS spectra of the three samples, α-HPG, C-HPG, and H-HPG (0.9%). The surface oxygen is categorized into three categories, including crystal lattice oxygen (O_I), vacancy oxygen (O_{II}), and adsorbed oxygen (O_{III}).[30−33] Moreover, the lattice oxygen corresponds to O^{2-} in calcium sulfate dihydrate, the vacant oxygen corresponds to the hydrophilic group −OH, and the adsorbed oxygen corresponds to the H_2O on the crystal surface. Figure 6b shows that the O 1s spectrum of the phosphogypsum reference group α-HPG consists of 12.20% O^{2-}, 58.29% −OH, and 29.51% H_2O, indicating that the hydration product of phosphogypsum contains a large number of hydrophilic groups −OH on the surface of the calcium sulfate dihydrate crystals, which is also one of the main reasons for the high water absorption rate of phosphogypsum. After adding the 10 wt % cement, 0.9 wt % H-PDMS to phosphogypsum, the content of −OH decreases by 0.98 and 2.19% and the lattice oxygen O^{2-} increases by 8.36 and 11.96%, respectively, indicating that the H-PDMS participates in the −OH polymerization reaction on the surface of phosphogypsum−cement crystals and adheres to the surface of the crystals, forming a continuous water-repellent film and improving its water resistance.

The adsorbed oxygen (O_{III}) is attributed to the adsorbed H_2O. After adding the 10 wt % cement, 0.9 wt % H-PDMS to phosphogypsum, the content of H_2O decreases by 7.38 and 9.77%, respectively, implying that the surface of the phosphogypsum crystal is coated with an organosilicon layer, which impedes the migration of free water and the attachment of water on the surface and reduces the hydration tendency of the modified phosphogypsum crystal surfaces when exposed to air.[34]

3.6. Pore Structure. The pore structures of the α-HPG and H-HPG are characterized by MIP, and the results are depicted in Figure 11. Figure 11a shows that the total intruded volume of α-HPG and H-HPG are 0.4131 and 0.4006 mL/g, respectively, indicating that the pore volume of the PG decreases by 3.03% after the cement and H-PDMS modification.

Figure 11b shows that the threshold pore size of the α-HPG and the H-HPG samples are 1053 and 1050 nm, respectively, which slightly decreases, but with little difference. However, in the range of 10−700 nm, the pore size distribution curves show a downward trend and move to pores with smaller sizes. The decrease of the water absorption rate is due to the decrease of total porosity, resulting in the increase of softening coefficient to some extent. The data of the pore structure of α-HPG and H-HPG are presented in Table 5, indicating that the cement and H-PDMS modification reduces the connectivity of the capillary pores and makes the pore structure dense.

3.7. Analysis of Surface Chemistry. The FTIR results of the samples are compared in Figure 12. The adsorption peaks at 3552 and 3407 cm^{-1} are ascribed to the symmetric stretch of crystal water in $CaSO_4·2H_2O$. The peak at 3606 cm^{-1} is ascribed to its antisymmetric stretch. The peaks near 1685 and 1621 cm^{-1} are attributed to the bending vibration of crystal water in hydrated gypsum. The absorption bands located in 1130 cm^{-1} are assigned to the antisymmetric stretch of SO_4^{2-}.[35] These peaks are also observed in the C-HPG and H-HPG samples, indicating that the hydrophobic modification does not alter the

https://doi.org/10.1021/acsomega.2c05662
ACS Omega 2022, 7, 41667−41677

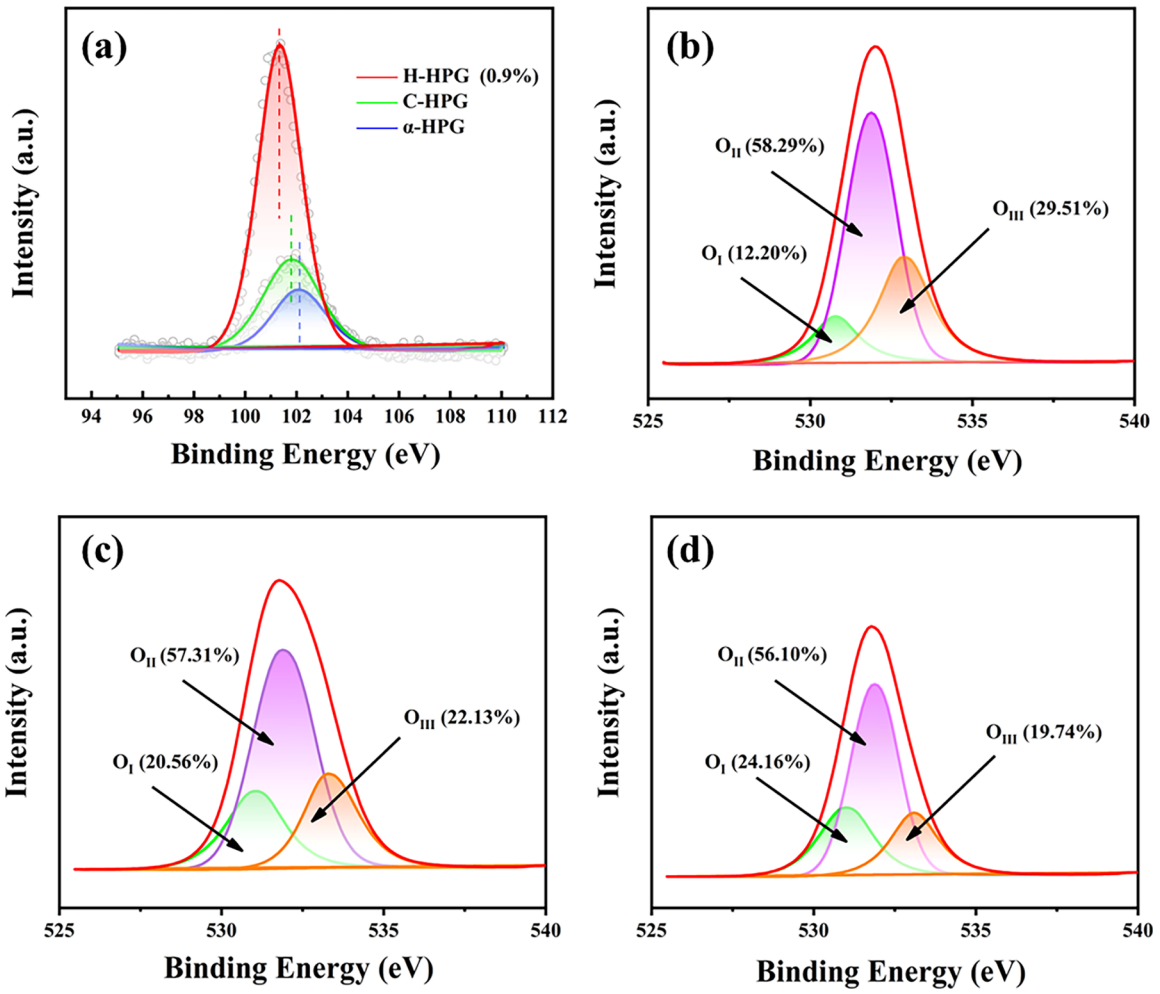

Figure 10. XPS spectra of Si 2p and O 1s in the HPG sample. (a) Change in Si 2p in three types of HPG samples. (b) Spectra of O 1s in α-HPC. (c) Spectra of O 1s in C-HPC. (d) Spectra of O 1s in H-HPC.

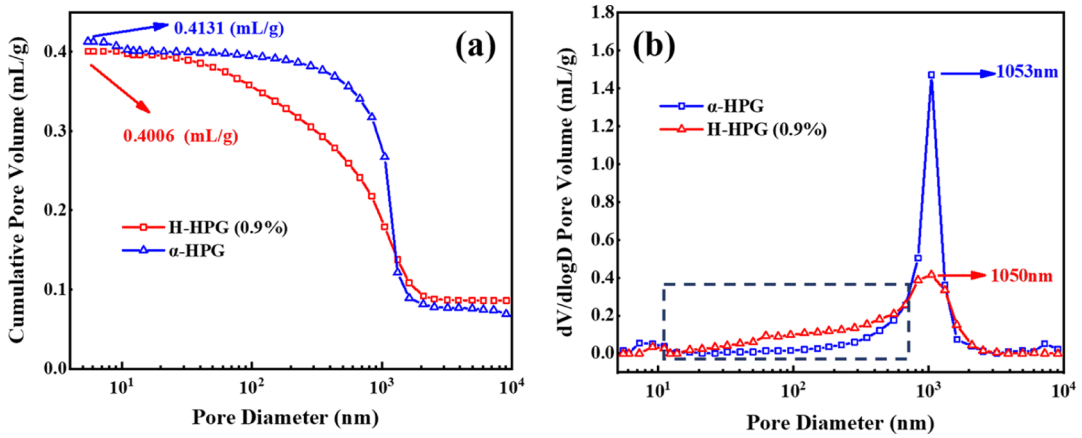

Figure 11. Effect of H-PDMS modification on (a) cumulative intrusion volume distribution and (b) pore size distribution.

Table 5. Pore Structure of Specimens

specimens	porosity (%)	total pore area (m^2/g)	average pore diameter (nm)	median pore diameter (nm)	total intrusion volume (mL/g)
α-HPG	47.88	7.543	219.1	1156.6	0.4131
H-HPG (0.9%)	43.67	7.365	217.6	938.8	0.4006

structure of the PG. However, compared with α-HPG and C-HPG, some new peaks appear in H-HPG owing to the hydrophobic modification of H-PDMS and cement.

The peaks at 2964 and 1363 cm^{-1} are attributed to the stretching vibration and symmetric deformation of $-CH_3$ in $-Si(CH_3)_2$ of PDMS. The peaks at 2927 and 2858 cm^{-1} are attributed to stretching vibration of asymmetric and symmetric stretch vibrations of methylene groups. The peak at 799 cm^{-1} is

https://doi.org/10.1021/acsomega.2c05662
ACS Omega 2022, 7, 41667−41677

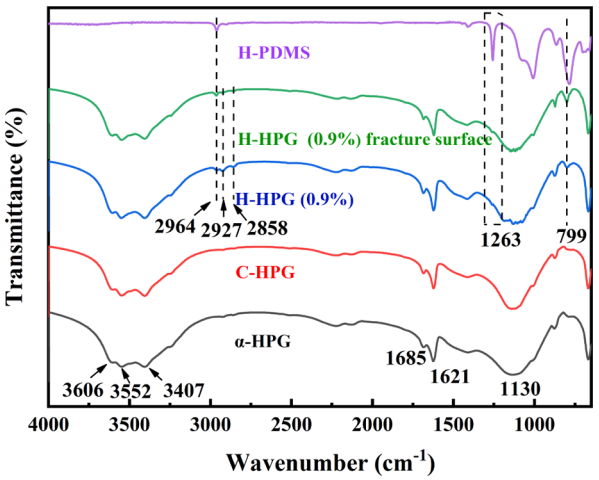

Figure 12. ATR-FTIR spectra of different sample surfaces.

attributed to the Si−O vibration. The blocks at 1130 cm^{-1} correspond to characteristic peaks of dihydrate.

The predicted chemical reactions between H-PDMS (including the curing agent and the accelerator) cement and phosphogypsum are illustrated in Figure 13. The cross-linking reaction of H-PDMS occurs under the action of an organotin catalyst (Sn-cat.) (Figure 13a).[36] The schematic sketch of the reaction is shown in Figure 13b. The hydration products of Portland cement are mainly calcium silicate hydrate (C−S−H) and calcium hydroxide (CH).[37,38] Under the alkaline environment provided by Portland cement hydration products, the curing agent TEOS is partially hydrolyzed to silanol.[39] Both of the hydroxyl groups of PDMS and silanol can react with the hydroxyl groups on the surface of C-HPG and bond on the surface of C-HPG by means of the Si−O bond. As a result, a H-PDMS layer is chemically bonded to the phosphogypsum-based composite from the inside out (Figure 13d). H-PDMS molecules which contain a large amount of methyl groups, completely cover the hydroxyl groups on the surface of 10% Portland cement-modified α-phosphogypsum, changing the phosphogypsum-based composite from hydrophilic to hydrophobic (Figure 13d).

3.8. Analysis of Different Kinds of HPG Micromorphology of the Hydration Product. The macro performances of specimens are determined by the composition of hydration products and their microstructure. Figure 14a−c shows the distribution of hydration products of the control sample α-HPG. Quite a few calcium sulfate dihydrate crystals are interconnected to form the network structure. The poor water resistance of gypsum is due to the weakness of contact points of calcium sulfate dihydrate.[40] The hydration reaction of phosphogypsum is as follows

$$CaSO_4 \cdot 0.5H_2O + 1.5H_2O = CaSO_4 \cdot 2H_2O \quad (3)$$

SEM images of C-HPG specimens with 10% Portland cement modification are shown in Figure 14d−f. The PG block product without cement has loose structure, large porosity, and the crystal morphology is mainly needle-like and sheet-like structures. With the addition of Portland cement, high-strength hydrated calcium aluminosilicate and ettringite are formed from

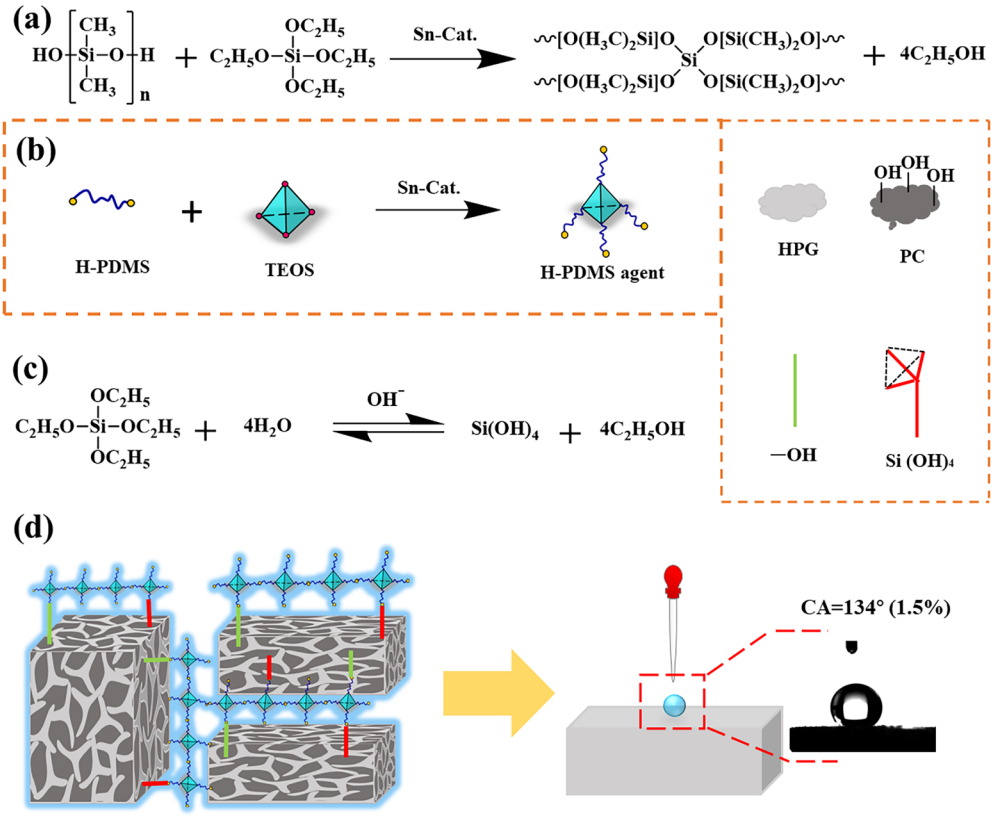

Figure 13. Schematic diagram of the chemical reaction. (a) Cross-linking reaction of H-PDMS occurs under the action of an organotin catalyst, (b) sketch of the H-PDMS cross-linking reaction, (c) TEOS hydrolyzes to silanol under an alkaline environment, and (d) phosphogypsum changes from hydrophilic to hydrophobic.

https://doi.org/10.1021/acsomega.2c05662
ACS Omega 2022, 7, 41667−41677

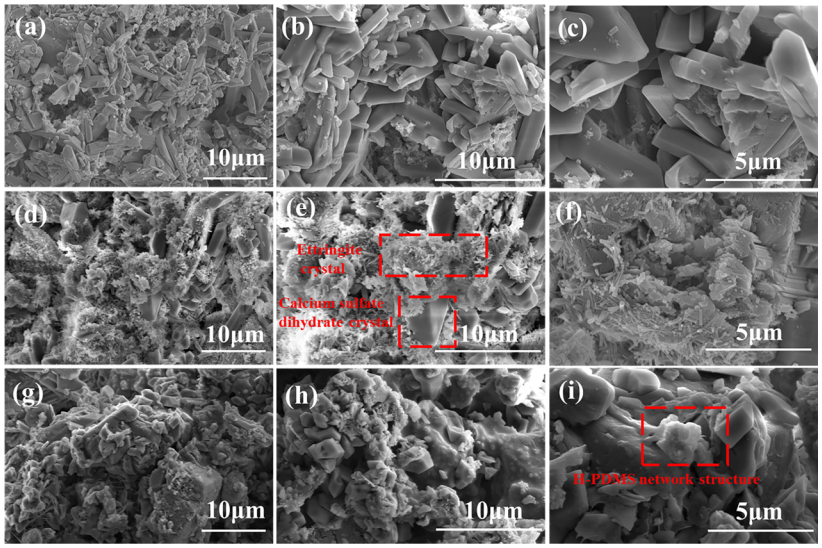

Figure 14. SEM images of specimens. (a–c) α-HPG at different magnifications, (d–f) C-HPG at different magnifications, and (g–i) H-HPG (0.9%) at different magnifications. (a,d,g) 3000×, (b,e,h) 5000×, and (e,f,i) 10,000×.

aluminosilicates in cement.[41] Aluminate in cement and gypsum form ettringite and the reaction is as follows

$$3CaO{\cdot}Al_2O_3 + 3(CaSO_4{\cdot}0.5H_2O) + 29.5H_2O = 3CaO{\cdot}Al_2O_3{\cdot}3CaSO_4{\cdot}31H_2O \quad (4)$$

The main hydration products of α-HPG (calcium sulfate dihydrate) are wrapped by cement hydration products mentioned above, on the surface of dihydrate gypsum crystals, and ettringite is interconnected with calcium sulfate dihydrate (Figure 14e), which significantly improves the softening coefficient of PG, filling the intercrystal voids to increase the density of the matrix and improving the compactness of specimens.[42] The addition of Portland cement not only improves the construction performance of PG but also provides phosphogypsum-based materials with −OH groups for the reaction with H-PDMS. SEM images of H-HPG (0.9%) are shown in Figure 14g–i. Figure 14i shows that a H-PDMS layer is chemically bonded to the surface of C-HPG, and cross-linked H-PDMS network structure mainly covers the surface of the C-HPG.

4. CONCLUSIONS

In summary, an integral hydrophobic phosphogypsum-based composite (H-HPG) was developed using H-PDMS as the organic waterproof admixture and Portland cement as the inorganic admixture, respectively. Herein, the mechanical strength, waterproof properties, surface chemistry, pore structure, and microstructure of different HPG samples were investigated. The results of this study can be summarized as follows:

(1) The fluidity of the different HPG mortar increased from 180 mm of α-HPG to 235 mm of H-HPG (1.5%), and the setting time prolonged after adding Portland cement and H-PDMS, from a final setting time of 27.5 min of α-HPG to 72 min of H-HPG (1.5%). In addition, both the compressive strength and flexural strength of the H-HPG modified with H-PDMS and Portland cement decreased. When the H-PDMS content was 1.5%, the flexural strength and compressive strength decreased by 40.00 and 33.63%, respectively, as compared with α-HPG. However, the toughness of the H-HPG improved with the modification of H-PDMS.

(2) With the increase of the H-PDMS agent contents from 0 to 1.5%, the water absorption of the hardened phosphogypsum–cement was decreased from 16.2 to 2.0%. The softening coefficient was improved to 0.94 when the dosage was 1.5%. The contact angle of phosphogypsum increased from 0 to 134° under the coupling effect of H-PDMS agents and cement.

(3) H-PDMS participated in the −OH polymerization reaction on the surface of phosphogypsum–cement crystals and adhered to the surface of the crystals. H-PDMS formed a chemically bonded layer on the surface of C-HPG, and the cross-linked H-PDMS hydrophobic network gave H-HPG an overall hydrophobicity. The modification of cement and H-PDMS reduced the porosity and made the pore structure denser. The porosity of H-HPG (0.9%) decreased by 8.79% compared to α-HPG, from 47.88 to 43.67%.

Hence, the H-PDMS- and Portland cement-modified phosphogypsum can be used in building materials with waterproof requirements, such as bathroom floor and phosphogypsum-based pavement that require the moisture resistance and coastal engineering projects. It is of great significance to accomplish the comprehensive utilization of solid waste phosphogypsum and solve its environmental pollution problems.

AUTHOR INFORMATION

Corresponding Author

Qibin Liu − *School of Materials and Metallurgy, Guizhou University, Guiyang 550025, P. R. China;* orcid.org/0000-0003-4387-4149; Email: qbliugzu@163.com

Authors

Guang Yang − *School of Materials and Metallurgy, Guizhou University, Guiyang 550025, P. R. China*

Lei Deng − *KZJ New Materials Group Guizhou Co., Ltd, Longli 551206, P. R. China*

https://doi.org/10.1021/acsomega.2c05662
ACS Omega 2022, 7, 41667−41677

Xiaofeng Luo − *KZJ New Materials Group Guizhou Co., Ltd, Longli 551206, P. R. China*

Complete contact information is available at: https://pubs.acs.org/10.1021/acsomega.2c05662

Funding

The research was supported by the Leizhi Innovation Fund (LETSGrp2020042401) from KZJ New Materials Group Guizhou Co., Ltd.

Notes

The authors declare no competing financial interest.

■ ACKNOWLEDGMENTS

The authors would like to thank the Shiyanjia lab (www.shiyanjia.com) for the XPS, MIP, and SEM tests.

■ REFERENCES

(1) Kouzbour, S.; Gourich, B.; Gros, F.; Vial, C.; Allam, F.; Stiriba, Y. Comparative analysis of industrial processes for cadmium removal from phosphoric acid: A review. *Hydrometallurgy* **2019**, *188*, 222−247.

(2) Sun, L.; Zhao, Z.; Yang, X.; Sun, Y.; Li, Q.; Luo, C.; Zhao, Q. Thermochemical decomposition of phosphogypsum with Fe-P slag via a solid-state reaction. *Chin. J. Chem. Eng.* **2021**, *47*, 113−119.

(3) Zhang, J.; Wang, X.; Jin, B.; Liu, C.; Zhang, X.; Li, Z. Effect of Soluble P_2O_5 Form on the Hydration and Hardening of Hemihydrate Phosphogypsum. *Adv. Mater. Sci. Eng.* **2022**, *2022*, 1212649.

(4) Chernysh, Y.; Plyatsuk, L.Environmentally friendly concept of phosphogypsum recycling on the basis of the biotechnological approach. *International Business, Trade and Institutional Sustainability*; Springer, 2020; pp 167−182.

(5) Lian, G.; Wang, B.; Lee, X.; Li, L.; Liu, T.; Lyu, W. Enhanced removal of hexavalent chromium by engineered biochar composite fabricated from phosphogypsum and distillers grains. *Sci. Total Environ.* **2019**, *697*, 134119.

(6) Huang, Y.; Xu, C.; Li, H.; Jiang, Z.; Gong, Z.; Yang, X.; Chen, Q. Utilization of the black tea powder as multifunctional admixture for the hemihydrate gypsum. *J. Clean. Prod.* **2019**, *210*, 231−237.

(7) Mu, Y.; Fu, Y. L.; Zhao, F. Q. Water-Resistant Modification of Desulphurization Gypsum Block. *Appl. Mech. Mater.* **2012**, *182*−*183*, 278−282.

(8) Jin, Z.; Ma, B.; Su, Y.; Lu, W.; Qi, H.; Hu, P. Effect of calcium sulphoaluminate cement on mechanical strength and waterproof properties of beta-hemihydrate phosphogypsum. *Constr. Build. Mater.* **2020**, *242*, 118198.

(9) Ma, P.; Li, S.; Cheng, B.; Yu, B.; Gao, Y.Effect of cement and fluidized bed combustion ashes on properties of phosphogypsum composite cementitious materials. *IOP Conference Series: Earth and Environmental Science*; IOP Publishing, 2021; Vol. *636*, p 012035.

(10) Meskini, S.; Samdi, A.; Ejjaouani, H.; Remmal, T. Valorization of phosphogypsum as a road material: Stabilizing effect of fly ash and lime additives on strength and durability. *J. Clean. Prod.* **2021**, *323*, 129161.

(11) Ou, Z. W.; Zhou, S. Y.; Xu, C. X.; Zhang, Y.; Yang, J. C.; Li, Y. X.Research and application of geopolymer cementitious material progress and review. *Applied Mechanics and Materials*; Trans Tech Publications, 2013; Vol. *405*−*408*, pp 2903−2911.

(12) Davidovits, J. Geopolymers and geopolymeric materials. *J. Therm. Anal.* **1989**, *35*, 429−441.

(13) Mashifana, T.; Sebothoma, J.; Sithole, T. Alkaline activation of basic oxygen furnace slag modified gold mine tailings for building material. *Adv. Civ. Eng.* **2021**, *2021*, 9984494.

(14) Lazorenko, G.; Kasprzhitskii, A.; Shaikh, F.; Krishna, R.; Mishra, J. Utilization potential of mine tailings in geopolymers: Physicochemical and environmental aspects. *Process Saf. Environ. Prot.* **2021**, *147*, 559−577.

(15) Li, X.; Zhao, Y.; Hu, Y.; Wang, G.; Xia, M.; Luo, B.; Luo, Z. Influence of Multiple Factors on the Workability and Early Strength Development of Alkali-Activated Fly Ash and Slag-Based Geopolymer-Stabilized Soil. *Materials* **2022**, *15*, 2682.

(16) Hamdane, H.; Tamraoui, Y.; Mansouri, S.; Oumam, M.; Bouih, A.; El Ghailassi, T.; Boulif, R.; Manoun, B.; Hannache, H. Effect of alkali-mixed content and thermally untreated phosphate sludge dosages on some properties of metakaolin based geopolymer material. *Mater. Chem. Phys.* **2020**, *248*, 122938.

(17) Zerfu, K.; Ekaputri, J. J. Review on alkali-activated fly ash based geopolymer concrete. *Mater. Sci. Forum* **2016**, *841*, 162−169.

(18) Nguyen, K. T.; Ahn, N.; Le, T. A.; Lee, K. Theoretical and experimental study on mechanical properties and flexural strength of fly ash-geopolymer concrete. *Constr. Build. Mater.* **2016**, *106*, 65−77.

(19) Li, Z.; Zhang, J.; Li, S.; Gao, Y.; Liu, C.; Qi, Y. Effect of different gypsums on the workability and mechanical properties of red mud-slag based grouting materials. *J. Clean. Prod.* **2020**, *245*, 118759.

(20) Shi, Y.; Cheng, L.; Tao, M.; Tong, S.; Yao, X.; Liu, Y. Using modified quartz sand for phosphate pollution control in cemented phosphogypsum (PG) backfill. *J. Clean. Prod.* **2021**, *283*, 124652.

(21) Wu, Q.; Ma, H.; Chen, Q.; Gu, B.; Li, S.; Zhu, H. Effect of silane modified styrene-acrylic emulsion on the waterproof properties of flue gas desulfurization gypsum. *Constr. Build. Mater.* **2019**, *197*, 506−512.

(22) Li, J.; Cao, J.; Ren, Q.; Ding, Y.; Zhu, H.; Xiong, C.; Chen, R. Effect of nano-silica and silicone oil paraffin emulsion composite waterproofing agent on the water resistance of flue gas desulfurization gypsum. *Constr. Build. Mater.* **2021**, *287*, 123055.

(23) Wang, F. F.; Li, G. Z.; Liu, M. R. Effect of waterproof emulsion on properties of calcined gypsum from flue gas desulfurization. *Adv. Mater. Res.* **2011**, *168*, 478−481.

(24) Jiang, Q.; Huang, J.; Ma, B.; Yang, Z.; Zhang, T. SiO_2/silicone hybrid superhydrophobic coating on gypsum-based materials with self-cleaning and moisture resistance. *J. Sol-Gel Sci. Technol.* **2020**, *96*, 207−218.

(25) Li, K.; Zeng, X.; Li, H.; Lai, X.; Xie, H. Effects of calcination temperature on the microstructure and wetting behavior of superhydrophobic polydimethylsiloxane/silica coating. *Colloids Surf., A* **2014**, *445*, 111−118.

(26) Ruan, S. Q.; Lin, C. Y.; Jiang, S. X.Study on the influence of polypropylene fiber and SBR latex on the static strength of rubber mortar. *Applied Mechanics and Materials*; Trans Tech Publications, 2013; Vol. *318*, pp 297−302.

(27) Wang, R.; Wang, P.-M.; Yao, L.-J. Effect of redispersible vinyl acetate and versatate copolymer powder on flexibility of cement mortar. *Constr. Build. Mater.* **2012**, *27*, 259−262.

(28) Li, J.; Guo, Z. Directional Penetration of Underwater Bubbles on Janus Surfaces. *Chem. Lett.* **2019**, *48*, 1254−1257.

(29) Zhang, Y.; Li, S.; Zhang, W.; Chen, X.; Hou, D.; Zhao, T.; Li, X. Preparation and mechanism of graphene oxide/isobutyltriethoxysilane composite emulsion and its effects on waterproof performance of concrete. *Constr. Build. Mater.* **2019**, *208*, 343−349.

(30) Tian, H.; Wan, D.; Che, Y.; Chang, J.; Zhao, J.; Hu, X.; Guo, Q.; Wang, Z.; Wang, L. Simultaneous magnesia regeneration and sulfur dioxide generation in magnesium-based flue gas desulfurization process. *J. Clean. Prod.* **2021**, *284*, 124720.

(31) Wang, H.; Xie, C. The effects of oxygen partial pressure on the microstructures and photocatalytic property of ZnO nanoparticles. *Phys. E* **2008**, *40*, 2724−2729.

(32) Wang, L.; Cheng, X.; Wang, Z.; Ma, C.; Qin, Y. Investigation on Fe-Co binary metal oxides supported on activated semi-coke for NO reduction by CO. *Appl. Catal., B* **2017**, *201*, 636−651.

(33) Wang, Q.; Chen, J.; Han, K.; Wang, J.; Lu, C. Influence of $BaCO_3$ on chlorine fixation, combustion characteristics and KCl conversion during biomass combustion. *Fuel* **2017**, *208*, 82−90.

(34) Yang, L.; Guan, B.; Wu, Z. Characterization and precipitation mechanism of α-calcium sulfate hemihydrate growing out of FGD gypsum in salt solution. *Sci. China, Ser. E: Technol. Sci.* **2009**, *52*, 2688−2694.

(35) Ru, X.; Ma, B.; Huang, J.; Huang, Y. Phosphogypsum transition to α-calcium sulfate hemihydrate in the presence of omongwaite in

NaCl solutions under atmospheric pressure. *J. Am. Ceram. Soc.* **2012**, *95*, 3478−3482.
(36) Yu, N.; Xiao, X.; Ye, Z.; Pan, G. Facile preparation of durable superhydrophobic coating with self-cleaning property. *Surf. Coat. Technol.* **2018**, *347*, 199−208.
(37) Barberena-Fernández, A.; Carmona-Quiroga, P. M.; Blanco-Varela, M. T. Interaction of TEOS with cementitious materials: Chemical and physical effects. *Cem. Concr. Compos.* **2015**, *55*, 145−152.
(38) Herb, H.; Gerdes, A.; Brenner-Weiß, G. Characterization of silane-based hydrophobic admixtures in concrete using TOF-MS. *Cem. Concr. Res.* **2015**, *70*, 77−82.
(39) Echeverría, J.; Moriones, P.; Arzamendi, G.; Garrido, J.; Gil, M.; Cornejo, A.; Martínez-Merino, V. Kinetics of the acid-catalyzed hydrolysis of tetraethoxysilane (TEOS) by 29Si NMR spectroscopy and mathematical modeling. *J. Sol-Gel Sci. Technol.* **2018**, *86*, 316−328.
(40) Zhou, P.-p.; Wu, H.-c.; Xia, Y.-m. Influence of synthetic polymers on the mechanical properties of hardened β-calcium sulfate hemihydrate plasters. *J. Ind. Eng. Chem.* **2016**, *33*, 355−361.
(41) Zhang, G.; Wu, C.; Hou, D.; Yang, J.; Sun, D.; Zhang, X. Effect of environmental pH values on phase composition and microstructure of Portland cement paste under sulfate attack. *Composites, Part B* **2021**, *216*, 108862.
(42) Evju, C.; Hansen, S. Expansive properties of ettringite in a mixture of calcium aluminate cement, Portland cement and β-calcium sulfate hemihydrate. *Cem. Concr. Res.* **2001**, *31*, 257−261.

https://doi.org/10.1021/acsomega.2c05662
ACS Omega 2022, 7, 41667−41677